# The Walker circulation, diabatic heating, and outgoing longwave radiation (Auxiliary Material)

Samuel N. Stechmann[1,2] and H. Reed Ogrosky[1]

[1]Department of Mathematics, University of Wisconsin, Madison, Wisconsin, USA.
[2]Department of Atmospheric and Oceanic Sciences, University of Wisconsin, Madison, Wisconsin, USA.

Geophysical Research Letters, 2014

## Contents



## 1 Materials and Methods

Three items of the Materials and Methods are described below: (i) the model for stationary wave patterns, (ii) the observational data, and (iii) the observational data analysis methods. Following these three items is a discussion of the current approach and a comparison with the methods of previous studies.

### 1.1 Model: stationary wave patterns

In this section, the derivations are outlined for the model equations for the stationary wave patterns, $K(x)$ and $R_m(x)$ for $m = 1, 2, 3, \cdots$. Parts of the derivation are classical [*Matsuno*, 1966; *Webster*, 1972; *Gill*, 1980], and parts are needed in order to describe the data analysis methods below. The main idea of the derivation is to reduce the three-dimensional $(x, y, z)$ equations to two-dimensional $(x, y)$ equations and finally to one-dimensional $(x)$ equations, using appropriate basis functions in the vertical $(z)$ and meridional $(y)$ coordinates [*Biello and Majda*, 2006; *Majda and Stechmann*, 2009; *Stechmann and Majda*, 2014].

The starting point is the set of linear long-wave equatorial primitive equations:

$$\begin{aligned} u_t - yv + p_x &= f^u \\ yu + p_y &= 0 \\ p_z &= \theta \\ u_x + v_y + w_z &= 0 \\ \theta_t + w &= f^\theta \end{aligned} \tag{S1}$$

Here $u$, $v$, and $w$ are the zonal, meridional, and vertical velocity anomalies, respectively; and $p$ and $\theta$ are the pressure and potential temperature, respectively. The zonal momentum source is $f^u$, and the potential temperature source is $f^\theta$. Due to the equatorial long-wave scaling, the time-tendency term $v_t$ of the meridional wind is neglected. The equations have been nondimensionalized using the standard equatorial reference scales [*Stechmann et al.*, 2008; *Majda and Stechmann*, 2009; *Stechmann and Majda*, 2014]. To obtain steady equations for the stationary wave patterns, the time tendency terms $u_t$ and $\theta_t$ will also be dropped below.

To arrive at a two-dimensional form of Eq. S1, vertical basis functions can be used to separate Eq. S1 into an infinite set of shallow water systems for the baroclinic modes. Here, only the first baroclinic mode is retained so that $u(x,y,z,t) = u(x,y,t)\sqrt{2}\cos(z)$, etc., with a slight abuse of notation in the re-use of symbol $u$. The resulting equations are

$$\begin{aligned} u_t - yv - \theta_x &= f^u \\ yu - \theta_y &= 0 \\ \theta_t - u_x - v_y &= f^\theta \end{aligned} \tag{S2}$$

which resemble the Matsuno–Gill model [*Matsuno*, 1966; *Gill*, 1980] except Eq. S2 includes no damping.

Finally, to arrive at a one-dimensional form of Eq. S2, meridional basis functions can be used to separate Eq. S2 into an infinite set of equations including the Kelvin wave $K(x)$ and long-wave equatorial Rossby waves $R_1(x), R_2(x), R_3(x), \cdots$. The natural meridional basis functions are the parabolic cylinder functions:

$$\phi_m(y) = \frac{1}{(m!\,\sqrt{\pi}\,2^m)^{1/2}}\, H_m(y)\, e^{-y^2/2}, \quad m = 0, 1, 2, \cdots \tag{S3}$$

where $H_m(y)$ are the Hermite polynomials:

$$H_m(y) = (-1)^m e^{+y^2} \frac{d^m}{dy^m} e^{-y^2}. \tag{S4}$$

For example, explicit formulas for the first few are

$$\phi_0(y) = \frac{1}{\pi^{1/4}}\, e^{-y^2/2} \tag{S5}$$

$$\phi_1(y) = \frac{1}{\pi^{1/4}} \frac{1}{\sqrt{2}}\, (2y)\, e^{-y^2/2} \tag{S6}$$

$$\phi_2(y) = \frac{1}{\pi^{1/4}} \frac{1}{2\sqrt{2}}\, (4y^2 - 2)\, e^{-y^2/2} \tag{S7}$$

The functions $\phi_m(y)$ form an orthonormal basis, and the variable $u(x,y)$ can then be expanded as

$$u(x,y) = \sum_{m=0}^{\infty} u_m(x)\, \phi_m(y) \tag{S8}$$

where the quantities $u_m(x)$ are obtained using the projection

$$u_m(x) = \int_{-\infty}^{\infty} u(x,y) \phi_m(y)\, dy \tag{S9}$$

Formulas analogous to Eqs. S8 and S9 also apply to $v, \theta, f^u, f^\theta$. Utilizing the projections in Eq. S9, the wave amplitudes $K(x)$ and $R_m(x)$ are defined as

$$K = \frac{1}{\sqrt{2}}(u_0 - \theta_0) \tag{S10}$$

$$R_m = \frac{\sqrt{m+1}}{\sqrt{2}}(u_{m+1} - \theta_{m+1}) - \frac{\sqrt{m}}{\sqrt{2}}(u_{m-1} + \theta_{m-1}), \quad m = 1, 2, 3, \cdots \tag{S11}$$

where $u_m$ and $\theta_m$ are the meridional projections from Eqs. S8 and S9. In addition, one can derive the following steady equations for the stationary wave patterns $K(x)$ and $R_m(x)$:

$$\frac{dK}{dx} = \frac{1}{\sqrt{2}}(f_0^u - f_0^\theta) \tag{S12}$$

$$\frac{dR_m}{dx} = (2m+1)v_m + \frac{\sqrt{m+1}}{\sqrt{2}}(f_{m+1}^u - f_{m+1}^\theta) + \frac{\sqrt{m}}{\sqrt{2}}(f_{m-1}^u + f_{m-1}^\theta), \quad m = 1, 2, 3, \cdots \tag{S13}$$

Note that the momentum source $f_0^u$ is relabelled as $F_{\text{mom}}$ and the heat source $f_0^\theta$ is relabelled as $F_{\text{heat}}$ in the main text for simplicity. Also note that meridional velocity $v_m$ enters into Eq. S13 in addition to the Rossby wave amplitude $R_m$ and the momentum and heat sources. Other formulations are also possible and Eq. S13 is used as a simple option. The variable $v_m$ is not a prognostic variable in the long-wave framework, and here it will be specified from observations, along with estimates of the observed source terms, in order to predict the wave amplitude $R_m$. The solutions of Eqs. S12–S13 are computed exactly using Fourier transforms.

Note that $K$ and $R_m$ ($m = 1, 2, \cdots$) denote the amplitudes of *structures* of Kelvin and Rossby waves; but $K$ and $R_m$ do *not* inherently contain in their definitions Eqs. S10–S11 any information about the *propagation* or *frequencies* of the structures. This latter information is specified in the equations of motion for the evolution of the structure in time. For instance, the temporal evolution of the amplitude $K(x,t)$ can be derived from Eq. S2 and is discussed below in Eq. S21. In other words, one can interpret $K$ and $R_m$ simply as new variables in a change of variables from "primitive variables" $u, v, \theta$ to "eigenmode variables" for each particular eigenmode structure.

To recover $u(x,y)$ from $K(x)$ and $R_m(x)$, $m = 1, 2, 3, \cdots$, the following formula is used:

$$u(x,y) = \frac{1}{\sqrt{2}}\left[K(x) - \frac{1}{2}R_1(x)\right]\phi_0(y) + \frac{1}{\sqrt{2}}\left[-\frac{1}{2\sqrt{2}}R_2(x)\right]\phi_1(y) + \sum_{m=2}^{\infty}\frac{1}{2\sqrt{2}}\left[\frac{1}{\sqrt{m}}R_{m-1}(x) - \frac{1}{\sqrt{m+1}}R_{m+1}(x)\right]\phi_m(y) \tag{S14}$$

where the series is truncated if only a finite number of Rossby wave amplitudes $R_m$ are used.

## 1.2 Data

To identify observational surrogates of the variables in Eqs. S1, S2, and S9–S13, two data sources are used here. First, as a surrogate for the heat source $f^\theta(x,y)$, NOAA interpolated outgoing longwave radiation (OLR) is used [*Liebmann and Smith*, 1996], along with the proportionality relationship in the main text. Interpolated OLR data is provided by the NOAA/OAR/ESRL PSD, Boulder, Colorado, USA, from their Web site at http://www.esrl.noaa.gov/psd/. Second, NCEP/NCAR reanalysis data is used for all other variables: wind, geopotential height, and sea surface temperature [*Kalnay et al.*, 1996]. NCEP Reanalysis data is provided by the NOAA/OAR/ESRL PSD, Boulder, Colorado, USA, from their Web site at http://www.esrl.noaa.gov/psd/. Both datasets have a horizontal spatial resolution of $2.5^\circ \times 2.5^\circ$ and a daily temporal resolution from 1 January 1979 to 31 December 2011.

To check the robustness of the results across different datasets, the NCEP/NCAR reanalysis data is compared with the ECMWF reanalysis data in Fig. S4. The ECMWF ERA40 reanalysis data spans the period of 1957–2002, and the ECMWF ERA–Interim reanalysis data spans the period of 1979–2013 [*Uppala et al.*, 2005]. In the recent 30-year period from 1980–2009, in Fig. S4, the NCEP/NCAR and ECMWF reanalyses show very similar patterns of $K(x)$ and $R_1(x)$, which lends confidence to the robustness of these reanalysis stationary wave patterns.

Also, while the reanalysis data has sometimes been refered to here as "observational" for simplicity, it is actually a combined product of observational data and model dynamics [*Kalnay et al.*, 1996; *Uppala et al.*, 2005]. Furthermore, satellite radiance data is assimilated to estimate temperature profiles, which

means the OLR and reanalysis data may not be completely independent data sources. To test the potential impact of satellite data on the reanalysis data, the earlier period of 1962–1968 is examined in Fig. S4; in this period, the reanalyses assimilate ample radiosonde data and no satellite data. While the Kelvin amplitude displays some noticeable differences, the general pattern is similar, and the Rossby amplitudes are all quite similar. Differences between the 1962–68 and 1980–2009 reanalysis product data could also be due to actual differences in the climate state during these two periods. In sum, this data comparison suggests that the large-scale patterns are relatively robust features of the mean climate state.

## 1.3 Methods: observational data analysis

In this section, a procedure is described to identify the wave amplitudes $K(x)$ and $R_m(x)$, $m = 1, 2, 3, \cdots$ from observational data. This procedure was recently introduced and described in detail elsewhere [*Stechmann and Majda*, 2014]. Here an overview of the procedure is described for the present focus on the Walker circulation, as opposed to the procedure's original focus of the Madden–Julian oscillation, which requires additional steps beyond what is needed here.

The method involves two steps that follow the path from Eq. S1 to Eq. S2 to Eqs. S12–S13: a vertical mode truncation to move from 3D $(x, y, z)$ to 2D $(x, y)$, and then a meridional mode truncation to move to 1D $(x)$. The first step distinguishes the overturning component of tropical circulations, which is characterized by opposing east–west winds in the lower troposphere (850 hPa) and upper troposphere (200 hPa). In the second step, the method furthermore breaks down the overturning circulation into its individual wave components, such as the Kelvin wave amplitude $K(x)$ and the equatorial Rossby wave amplitudes $R_m(x)$. From these two steps, this method allows a more direct comparison of observations and theory than previously possible.

First, to define the first baroclinic mode variables $u(x, y)$, $v(x, y)$, and $\theta(x, y)$ from (S2), a simple method is used here. The method utilizes data from only two pressure levels, 850 and 200 hPa, in order to capture the essence of the first baroclinic mode structure:

$$u(x,y) = \frac{\mathrm{U850}(x,y) - \mathrm{U200}(x,y)}{2\sqrt{2}} \tag{S15}$$

$$v(x,y) = \frac{\mathrm{V850}(x,y) - \mathrm{V200}(x,y)}{2\sqrt{2}} \tag{S16}$$

$$\theta(x,y) = -\frac{\mathrm{Z850}(x,y) - \mathrm{Z200}(x,y)}{2\sqrt{2}} \tag{S17}$$

where $Z$ is geopotential height and is related to potential temperature via the hydrostatic balance equation. This formulation is a crude, Boussinesq-like representation of the vertical modes that can be derived from the primitive equations or the anelastic equations [*Kasahara*, 1976; *Kasahara and Puri*, 1981; *Fulton and Schubert*, 1985]. The equations have been nondimensionalized using the standard equatorial reference scales [*Stechmann et al.*, 2008; *Majda and Stechmann*, 2009; *Stechmann and Majda*, 2014]. By taking the difference between the data at 850 and 200 hPa, this method isolates the overturning component of tropical circulations from the barotropic component.

Second, to define the equatorial wave amplitudes $K(x)$ and $R_m(x)$, the definitions in (S10)–(S11) utilize projections of $u(x, y)$ and $\theta(x, y)$ onto meridional basis functions. The projection in (S9) is performed discretely as a Riemann sum. While the theoretical description above applies to an equatorial $\beta$-plane with $-\infty < y < +\infty$, the data analysis must use latitude on a sphere. To relate latitude and meridional length, a simple correspondence is used here: $1^\circ$ latitude $\approx 110$ km.

The pattern correlation is used here to compare observed and modeled data; for a comparison of two functions $f(x)$ and $g(x)$, it is defined as

$$PC(f,g) = \frac{\frac{1}{L}\int_0^L f(x)g(x)\,dx}{\left[\frac{1}{L}\int_0^L |f(x)|^2\,dx\right]^{1/2}\left[\frac{1}{L}\int_0^L |g(x)|^2\,dx\right]^{1/2}} \tag{S18}$$

and it takes values in the range of -1 to 1.

## 1.4 Comparison with methods of previous studies

At the end of section 3.1 of the main text, it was noted that the approach here differs from previous common approaches in several ways. In this section, many aspects are discussed in further detail, including several subtleties:

- Damping and its role as a surrogate
- The $k = 0$ mode, damping, and a mathematical subtlety
- Interpretation of steady undamped wave patterns
- Distinguishing the first baroclinic mode
- Distinguishing the equatorial wave types
- Diabatic heating rate estimates and their zonal variations

### Damping and its role as a surrogate

Since damping is not included in the models used here, whereas it is normally included in Matsuno–Gill-type models, we now describe some justifications for including or not including damping.

In terms of physical processes, the forcing terms $f^u$ and $f^\theta$ in Eq. S2 should represent (among other things) momentum forcing, such as convective momentum transport, and heat sources and sinks, such as radiative heating and cooling. If accurate observational estimates are known, then one could simply prescribe the functions $f^u(x, y, t)$ and $f^\theta(x, y, t)$ using these observational estimates. However, accurate observational estimates have traditionally not been available, which heightens the appeal of another option: to use a model for $f^u$ and $f^\theta$.

Several options exist for modeling these processes. As a comprehensive option, for instance, one could use a radiative transfer algorithm. Such algorithms are quite complex, in contrast to the dynamical core of Matsuno–Gill-type models, which suggests the consideration of simpler models of radiative transfer. A very simple option is to model radiative forcing using a damping term—i.e., Newtonian cooling. Such a choice requires justification, perhaps based on physical principles or based on a simplification of the equations for comprehensive radiative transfer. In any case, damping is a modeling option.

Returning now to the original motivation, the goal is to represent the forcing terms $f^u$ and $f^\theta$ in Eq. S2, and two main options exist: (i) prescribe them using observational estimates, or (ii) model them. (Or perhaps a third option is to use a combination of the two.) The present paper tests the following hypothesis: In modeling the Walker circulation, the forcing terms can be prescribed from observational estimates alone, using $f^u \approx 0$ and $f^\theta \propto$ OLR. Using this approach, excellent agreement is found between the undamped model and the observed Walker circulation.

This does not necessarily mean that Rayleigh friction and Newtonian cooling should never be used. For the present application, however, they do not appear to be needed.

### The $k = 0$ mode, damping, and a mathematical subtlety

An important element of the present model is that it does not include the $k = 0$ mode (also called the zonally uniform or zonally symmetric component). The $k = 0$ mode introduces a mathematical subtlety involving damping, and this subtlety does not seem to be well known.

The mathematical subtlety involves two points. First, the undamped model (in a steady state) in Eq. S2 has a solution only if $f^u$ and $f^\theta$ satisfy certain consistency conditions. This has been pointed out by *Majda and Klein* [2003]. Specifically, it is the zonally uniform components, $\overline{f^u}$ and $\overline{f^\theta}$, that must satisfy certain consistency conditions. Second, the forcing introduced by *Gill* [1980] does not satisfy the consistency conditions.

What is the consequence of using forcing terms $f^u$ and $f^\theta$ that do not satisfy the consistency conditions? One consequence is that the weak damping limit causes the zonally uniform circulation to become very

strong—in fact, infinitely strong. To see the consequences in a simple setting, consider the steady, forced Kelvin wave in Eq. S12 with damping added:

$$\frac{dK}{dx} = \frac{1}{\sqrt{2}}(f_0^u - f_0^\theta) - \frac{1}{\tau}K, \tag{S19}$$

which assumes equal momentum and thermal damping rates for simplicity. The solution for the zonally uniform component $\bar{K}$ is then given by

$$\bar{K} = \tau \cdot \frac{\overline{f_0^u} - \overline{f_0^\theta}}{\sqrt{2}}. \tag{S20}$$

If damping is weak (i.e., $\tau$ is large), then $\bar{K}$ can be very large. In fact, $\bar{K}$ becomes infinite in the limit as $\tau \to \infty$. In contrast, the zonally varying component of $K(x)$ remains finite as $\tau$ is increased. Consequently, if damping is weak, the zonally uniform component of the circulation can become the dominant feature of the flow.

Such consequences have been seen in some previous studies [*Wu et al.*, 2001], and they could be avoided in several ways. As one option, one could apply sufficiently strong damping to achieve a zonally uniform circulation of a reasonable magnitude; this option would also impose strong damping upon the zonally varying cicrulation. As another option, one could choose forcing functions that satisfy the consistency conditions, unlike the forcing of *Gill* [1980]. For instance, in the case of the Kelvin wave example in Eqs. S19–S20, the consistency condition is $\overline{f_0^u} = \overline{f_0^\theta}$. As a third option, one could choose not to model the zonally uniform component of the circulation. In other words, one could satisfy the consistency conditions in a trivial way by choosing forcing functions that satisfy $\overline{f^u} = \overline{f^\theta} = 0$. This option avoids all of the subtle issues described above, and it is the approach used in the present paper.

**Interpretation of steady undamped wave patterns**

The concept of a "steady wave pattern" may seem somewhat counterintuitive, since waves oscillate and propagate. Two interpretations are now described to clarify the meaning here. The steady wave patterns could be interpreted as either (i) the temporal average of an unsteady wave equation, or (ii) the steady state that would be achieved in a damped model in the limit that the damping rate tends to zero.

The first potential interpretation is that a steady wave pattern is a temporal average of the unsteady undamped equation for Kelvin waves, which is

$$\frac{\partial K}{\partial t} + \frac{\partial K}{\partial x} = f^K, \tag{S21}$$

where the forcing $(f_0^u - f_0^\theta)/\sqrt{2}$ has been denoted by $f^K$ to ease notation. A temporal average of this equation from $t = 0$ to $t = T$ leads to

$$\frac{K(x,T) - K(x,0)}{T} + \partial_x \langle K \rangle = \langle f^K \rangle, \tag{S22}$$

where $\langle f \rangle$ denotes the time average: $\langle f \rangle = \frac{1}{T}\int_0^T f(x,t)\, dt$. For large $T$, this equation becomes

$$\partial_x \langle K \rangle \approx \langle f^K \rangle, \tag{S23}$$

which is essentially the same as Eq. 6 from the main text, and which corresponds to an undamped "steady state." While this is not a true deterministic steady state, it is a statistical steady state in the sense that the time-averaged variables will satisfy this relationship. Through the temporal average, the influence of propagating Kelvin waves is averaged out, leaving only the steady Kelvin wave pattern described in the main text.

The second interpretation is that a steady (undamped) wave pattern is the steady state that would be achieved in a damped model in the limit that the damping rate tends to zero. The damped version of Eq. S21 is given by

$$\frac{\partial K}{\partial t} + \frac{\partial K}{\partial x} = -\frac{1}{\tau}K + f^K, \tag{S24}$$

where initial condition $K(x,0)$ could be specified. The solution in Fourier space is found by assuming the expansion $K(x,t) = \sum_k \hat{K}_k(t) \exp(ikx)$, which leads to

$$\frac{d\hat{K}_k}{dt} = -(ik + \tau^{-1})\hat{K}_k + \hat{f}_k^K. \tag{S25}$$

This is a linear ordinary differential equation that can be solved exactly for $\hat{K}_k(t)$ at any time $t$, from which $K(x,t)$ can be obtained by an inverse Fourier transform. A steady state solution is then obtained by taking the limit as $t \to \infty$; it is given by

$$\hat{K}_k = \frac{\hat{f}_k^K}{ik + \tau^{-1}}. \tag{S26}$$

In the limit of weak damping (i.e., as $\tau^{-1} \to 0$),

$$\hat{K}_k \to \frac{\hat{f}_k^K}{ik} \qquad \text{as} \qquad \tau^{-1} \to 0. \tag{S27}$$

This is precisely the Fourier transform of Eq. 6 of the main text, which can hence be interpreted as the steady state that would be achieved in a damped model, in the limit that the damping rate tends to zero. This is a regular limit in the setup used here, although in other cases the limit can potentially be subtle, since certain consistency conditions must be satisfied by the forcing in the undamped limit, as pointed out by *Majda and Klein* [2003]. The subtlety arises only for the zonally uniform component ($k = 0$ mode), since a potential singularity can arise in this limit if $k = 0$ and $\tau^{-1} \to 0$. In the present paper, this subtlety is not an issue, since the zonally uniform component is not considered.

Finally, we note that the notion of a "steady wave" is also commonly used for circulation patterns outside the tropics. For example, see Chapter 6 of *James* [1995] on barotropic steady waves forced by topography. Other terminology is also sometimes used interchangeably, such as "steady eddies" or "stationary waves."

**Distinguishing the first baroclinic mode**

In the results of the present paper, a new observational data analysis method has been used [*Stechmann and Majda*, 2014]. One important feature of the method is that it distinguishes the overturning component of tropical circulations—i.e., the first vertical baroclinic mode. The first baroclinic mode is characterized by opposing zonal winds in the lower troposphere (850 hPa) and upper troposphere (200 hPa), as indicated in the schematic diagram in Fig. 1a. It is this vertical mode that is typically represented in simple models of the Walker circulation, as in the present paper. Consequently, if the first baroclinic mode can be isolated in observational data (as is attempted in the new observational data analysis method), it should provide the most direct comparison between model and observations.

In contrast, it is traditional to analyze observational data at a single pressure level, such as 850 hPa, in which case the fluctuations are caused by a superposition of numerous vertical modes (such as other baroclinic modes and the barotropic mode). Hence one cannot expect to see excellent agreement between a first-baroclinic-mode model and observations at a single pressure level.

Some have expressed concern about the use of vertical internal modes in modeling the tropical atmosphere (e.g., see [*Lindzen*, 2003] and references therein). On the other hand, *Chumakova et al.* [2013] have presented a theoretical argument to justify the use of vertical modes. The results of the present paper are perhaps a posteriori evidence of the utility of the vertical mode perspective.

**Distinguishing the equatorial wave types**

As another feature, the methods here break down the overturning circulation into its individual wave components, such as the Kelvin wave amplitude $K(x)$ and the equatorial Rossby waves, $R_m(x)$. In so doing, it does not consider the momentum forcing $f^u$ and diabatic heating $f^\theta$ separately. Instead, they are considered together through the quantities $f^u \pm f^\theta$, as seen in Eqs. S12–S13. In so doing, the strengths of $f^u$ and $f^\theta$ are considered relative to each other, and $f^u$ is assumed to be small not in an absolute sense but in relation to the strong diabatic heating variations, $f^\theta$.

**Diabatic heating rate estimates and their zonal variations**

Two aspects of the diabatic heating are treated differently here than in many previous studies. First, in estimating a relationship between OLR and diabatic heating, the $k = 0$ mode of OLR has been removed. This is in contrast to previous estimates of such a relationship [*Christy*, 1991; *Yanai and Tomita*, 1998]. Second, diabatic heating variations are considered here across the global tropics, rather than a local diabatic heat source as popularized by *Gill* [1980].

# References


Biello, J. A., and A. J. Majda (2006), Modulating synoptic scale convective activity and boundary layer dissipation in the IPESD models of the Madden–Julian oscillation, *Dyn. Atmos. Oceans*, *42*, 152–215.

Christy, J. R. (1991), Diabatic heating rate estimates from European Centre for Medium-Range Weather Forecasts analyses, *J. Geophys. Res.*, *96*(D3), 5123–5135.

Chumakova, L. G., R. R. Rosales, and E. G. Tabak (2013), Leaky rigid lid: New dissipative modes in the troposphere, *J. Atmos. Sci.*, *70*(10), 3119–3127.

Fulton, S. R., and W. H. Schubert (1985), Vertical normal mode transforms: Theory and application, *Mon. Wea. Rev.*, *113*(4), 647–658.

Gill, A. E. (1980), Some simple solutions for heat-induced tropical circulation, *Q. J. Royal Meteor. Soc.*, *106*(449), 447–462.

James, I. N. (1995), *Introduction to Circulating Atmospheres*, Cambridge Atmospheric and Space Science Series, Cambridge University Press.

Kalnay, E., M. Kanamitsu, R. Kistler, W. Collins, D. Deaven, L. Gandin, M. Iredell, S. Saha, G. White, J. Woollen, et al. (1996), The NCEP/NCAR 40-year reanalysis project, *Bull. Amer. Meteor. Soc.*, *77*(3), 437–471.

Kasahara, A. (1976), Normal modes of ultralong waves in the atmosphere, *Mon. Wea. Rev.*, *104*(6), 669–690.

Kasahara, A., and K. Puri (1981), Spectral representation of three-dimensional global data by expansion in normal mode functions, *Mon. Wea. Rev.*, *109*(1), 37–51.

Liebmann, B., and C. A. Smith (1996), Description of a complete (interpolated) outgoing longwave radiation dataset, *Bull. Amer. Meteor. Soc.*, *77*, 1275–1277.

Lindzen, R. S. (2003), The interaction of waves and convection in the tropics, *J. Atmos. Sci.*, *60*(24), 3009–3020.

Majda, A. J., and R. Klein (2003), Systematic multiscale models for the Tropics., *J. Atmos. Sci.*, *60*, 393–408.

Majda, A. J., and S. N. Stechmann (2009), The skeleton of tropical intraseasonal oscillations, *Proc. Natl. Acad. Sci. USA*, *106*(21), 8417–8422.

Matsuno, T. (1966), Quasi-geostrophic motions in the equatorial area, *J. Meteor. Soc. Japan*, *44*(1), 25–43.

Stechmann, S. N., and A. J. Majda (2014), Identifying the skeleton of the Madden–Julian oscillation in observational data, *Mon. Wea. Rev.*, p. in press.

Stechmann, S. N., A. J. Majda, and B. Khouider (2008), Nonlinear dynamics of hydrostatic internal gravity waves, *Theor. Comp. Fluid Dyn.*, *22*, 407–432.

Uppala, S. M., P. W. Kållberg, A. J. Simmons, U. Andrae, V. Bechtold, M. Fiorino, J. K. Gibson, J. Haseler, A. Hernandez, G. A. Kelly, et al. (2005), The ERA-40 re-analysis, *Q. J. Roy. Meteor. Soc.*, *131*(612), 2961–3012.

Webster, P. J. (1972), Response of the tropical atmosphere to local, steady forcing, *Mon. Wea. Rev.*, *100*(7), 518–541.

Wu, Z., E. S. Sarachik, and D. S. Battisti (2001), Thermally driven tropical circulations under Rayleigh friction and Newtonian cooling: Analytic solutions, *J. Atmos. Sci.*, *58*(7), 724–741.

Yanai, M., and T. Tomita (1998), Seasonal and interannual variability of atmospheric heat sources and moisture sinks as determined from NCEP-NCAR reanalysis, *J. Climate*, *11*(3), 463–482.

## 2 Supplementary Figures

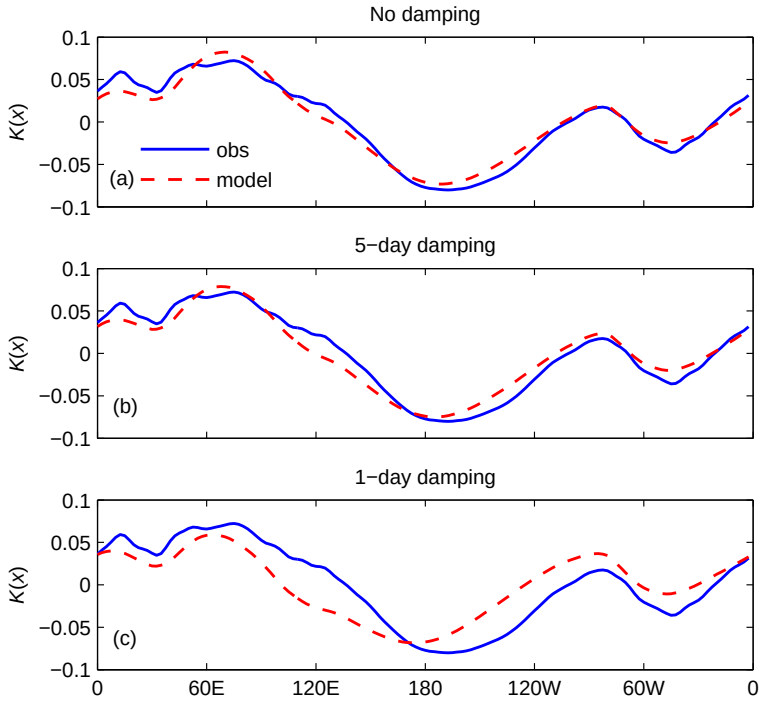


Figure S1: (a) Same as Figure 1c, which is undamped, repeated here for ease of comparison. (b) Same as Figure 1c, except with model damping time scale of 5 days. (b) Same as Figure 1c, except with model damping time scale of 1 day. Damped solutions are computed using Eqn. S19.

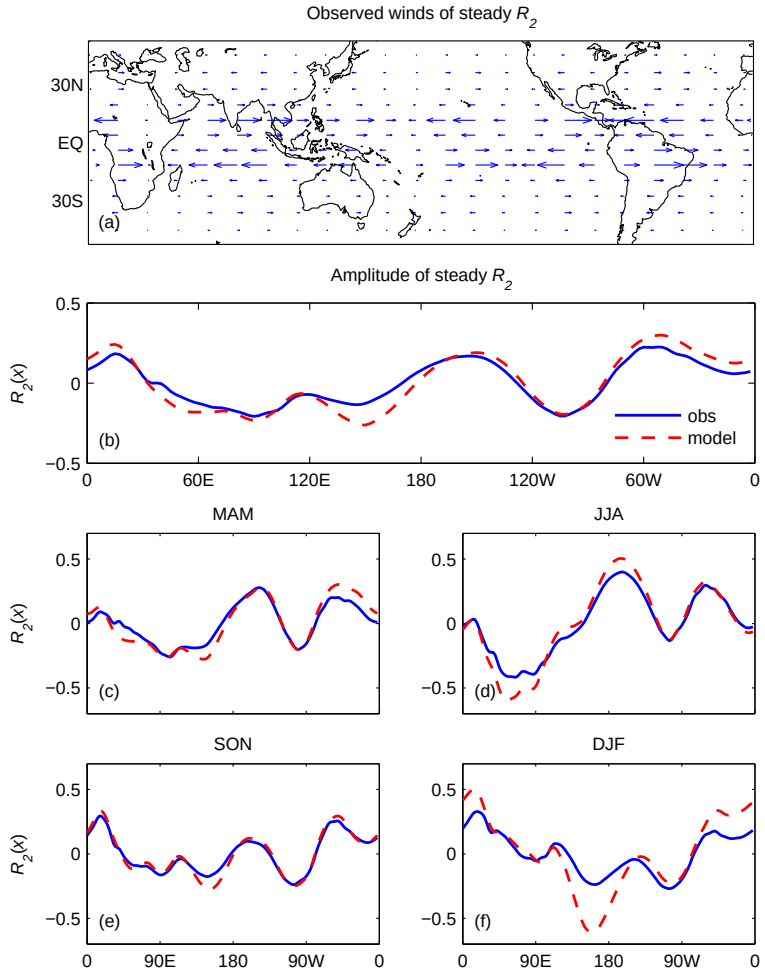


Figure S2: (a) The zonal winds of Rossby wave $R_2$ as observed in NCEP/NCAR reanalysis data, averaged from 1980-2009. (b) The amplitude of the observed (solid blue line) and model-predicted (dashed red line) $R_2$ averaged from 1980-2009, and also averaged seasonally for the (c) MAM, (d) JJA, (e) SON, and (f) DJF seasons.

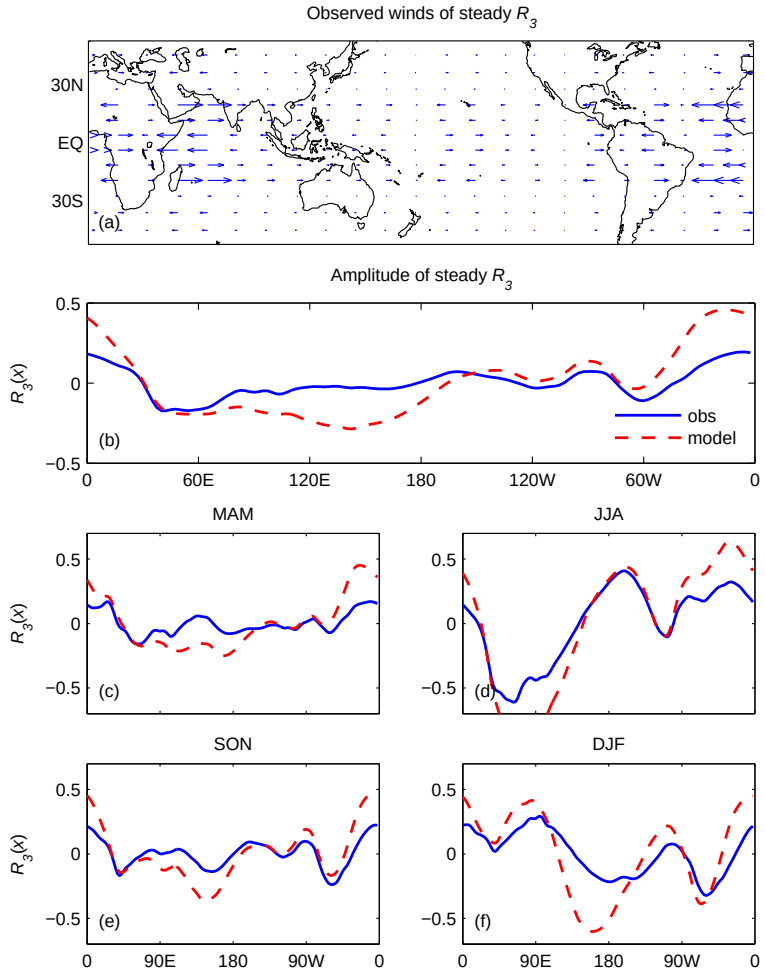


Figure S3: (a) The zonal winds of Rossby wave $R_3$ as observed in NCEP/NCAR reanalysis data, averaged from 1980-2009. (b) The amplitude of the observed (solid blue line) and model-predicted (dashed red line) $R_3$ averaged from 1980-2009, and also averaged seasonally for the (c) MAM, (d) JJA, (e) SON, and (f) DJF seasons.

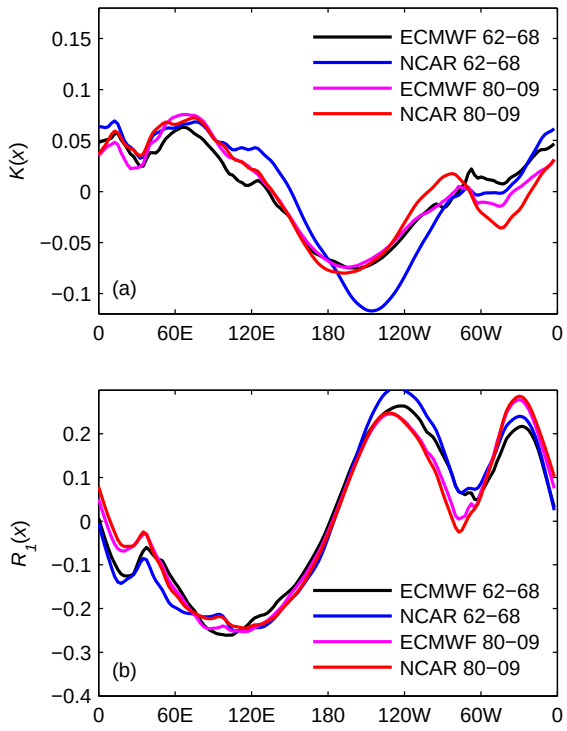


Figure S4: (a) Comparison of Kelvin amplitude $K(x)$ for different reanalysis datasets and time periods: NCEP/NCAR 1980–2009 (red), ECMWF 1980–2009 (magenta), NCEP/NCAR 1962–1968 (blue), ECMWF 1962–1968 (black). (b) Same as (a) except for Rossby wave amplitude $R_1(x)$.